

# Aviation 2006 NO<sub>x</sub>-induced effects on atmospheric ozone and HO<sub>x</sub> in Community Earth System Model (CESM)

A. Khodayari<sup>1</sup>, S. Tilmes<sup>3</sup>, S. C. Olsen<sup>2</sup>, D. B. Phoenix<sup>2</sup>, D. J. Wuebbles<sup>2</sup>, J.-F. Lamarque<sup>3</sup>, C.-C. Chen<sup>3</sup>

[1] {Department of Civil and Environmental Engineering, University of Illinois at Urbana-Champaign, Urbana, IL 61801, USA}

[2] {Department of Atmospheric Sciences, University of Illinois at Urbana-Champaign, Urbana, IL 61801, USA}

[3] {National Center for Atmospheric Research, Boulder, CO, USA}

Correspondence to: Donald J. Wuebbles (wuebbles@illinois.edu)

## Abstract

The interaction between atmospheric chemistry and ozone (O<sub>3</sub>) in the upper troposphere and lower stratosphere (UTLS) presents a major uncertainty in understanding the effects of aviation on climate. In this study, two configurations of the atmospheric model from the Community Earth System Model (CESM), CAM4 and CAM5, are used to evaluate the effects of aircraft nitrogen oxide (NO<sub>x</sub>=NO+NO<sub>2</sub>) emissions on ozone and the background chemistry in the UTLS. CAM4 and CAM5 simulations were both performed with extensive tropospheric and stratospheric chemistry including 133 species and 330 photochemical reactions. CAM5 includes direct and indirect aerosol effects on clouds using a modal aerosol module (MAM) whereby CAM4 uses a bulk aerosol module, which can only simulate the direct effect. To examine the accuracy of the aviation NO<sub>x</sub> induced ozone distribution in the two models, results from the CAM5 and CAM4 simulations are compared to ozonesonde data. Aviation NO<sub>x</sub> emissions for 2006 were obtained from the AEDT (Aviation Environmental Design Tool) global commercial aircraft emissions inventory. Differences between simulated O<sub>3</sub> concentrations and ozonesonde measurements averaged at representative levels in the

1 troposphere and different regions are 13% in CAM5 and 18% in CAM4. Results show a  
2 localized increase in aviation induced O<sub>3</sub> concentrations at aviation cruise altitudes that  
3 stretches from 40°N to the North Pole. The results indicate a greater and more disperse  
4 production of aviation NO<sub>x</sub>-induced ozone in CAM5, with the annual tropospheric mean O<sub>3</sub>  
5 perturbation of 1.2 ppb (2.4%) for CAM5 and 1.0 ppb (1.9%) for CAM4. The annual mean O<sub>3</sub>  
6 perturbation peaks at about 8.2 ppb (6.4%) and 8.8 ppb (5.2%) in CAM5 and CAM4,  
7 respectively. Aviation emissions also result in increased OH concentrations and methane  
8 (CH<sub>4</sub>) loss rates, reducing the tropospheric methane lifetime in CAM5 and CAM4 by 1.69%  
9 and 1.40%, respectively. Aviation NO<sub>x</sub> emissions are associated with an instantaneous change  
10 in global mean short-term O<sub>3</sub> radiative forcing (RF) of 40.3 and 36.5 mWm<sup>-2</sup> in CAM5 and  
11 CAM4, respectively.

## 12 **1 Introduction**

13 The aviation industry has grown rapidly since its nascence, at a rate of 9% per year for  
14 passenger traffic between 1960 and 2000 (IPCC, 1999) and is one of the fastest growing  
15 transportation sectors (IPCC, 2007). Despite several international economic and other setbacks  
16 over the last few decades, including large price increases for fuel, and a global recession, the  
17 aviation industry continues to experience growth. The 2013 FAA forecast calls for an annual  
18 average increase of 2.2% per year in U.S. passenger carrier growth over the next twenty years.  
19 The growth is predicted to be slightly greater for the first five years under the assumption of a  
20 faster U.S. economic growth rate (FAA, 2013). As such, it is important to assess the potential  
21 impacts that aviation will have on future climate.

22 Aviation affects climate in various ways. The main concerns to climate result from the  
23 emissions of carbon dioxide (CO<sub>2</sub>) and nitrogen oxides (NO<sub>x</sub>=NO+NO<sub>2</sub>), which influence the  
24 gas-phase and aerosol chemistry. Other aviation induced impacts result from the emissions of  
25 H<sub>2</sub>O, and the emission of sulfate and soot particles, which influence the formation of contrail-  
26 cirrus clouds and change the cloudiness by acting as cloud condensation nuclei (e.g., Gettelman  
27 et. al., 2012). The resulting effects of these emissions modify the chemical properties of the  
28 upper troposphere and lower stratosphere and the cloud microphysics that affect the Earth's  
29 climate system radiative forcing. For the majority of these effects, the radiative forcing is

1 positive; however, for sulfate particles—which reflect incoming shortwave radiation, and for  
2 the increases in OH concentrations—which reduce the CH<sub>4</sub> concentrations, the radiative  
3 forcing is negative (Lee et al., 2009). The indirect effect of sulfate aerosols may, on the other  
4 hand, result in a negative radiative forcing via liquid clouds which dominates the warming  
5 caused from contrails and black carbon (BC) emissions (Gettelman et al., 2013). This study  
6 will focus on the aviation NO<sub>x</sub>-induced effects, and particularly the NO<sub>x</sub>-induced effect on  
7 atmospheric ozone (O<sub>3</sub>).

8 There have been many previous studies that examined the effect of aviation NO<sub>x</sub> emissions on  
9 NO<sub>x</sub>-induced O<sub>3</sub> (e.g., Derwent et al., 1999; Fuglestedt et al., 1999; Wild et al., 2001;  
10 Derwent et al., 2001; Stevenson and Doherty, 2004; Köhler et al., 2008; Hoor et al., 2009;  
11 Koffi et al., 2010; Hodnebrog et al., 2011). The aviation NO<sub>x</sub>-induced changes in O<sub>3</sub> calculated  
12 in these studies varies between 0.46 to 0.90 Dobson units of ozone per TgN per year  
13 (DU(O<sub>3</sub>)/[TgN/yr]). Other recent studies have examined the factors that control the production  
14 of NO<sub>x</sub>-induced O<sub>3</sub>. Stevenson and Derwent (2009) found that the O<sub>3</sub> and CH<sub>4</sub> response to  
15 NO<sub>x</sub> emissions varies regionally, and are most sensitive in regions with low background NO<sub>x</sub>  
16 concentrations. Several studies analyzed the impact of the location and time of the emissions  
17 (Derwent et al., 2001; Stevenson et al., 2004). Derwent et al. (2001) analyzed the changes in  
18 methane and tropospheric ozone after emitting pulses of NO<sub>x</sub> at the surface and upper  
19 troposphere in both the northern and southern hemispheres and found that while the changes in  
20 methane radiative forcing were dominated by methane emissions, changes in tropospheric  
21 ozone radiative forcing were dominated by changes in ozone precursor gases, notably NO<sub>x</sub>  
22 emissions. Stevenson et al. (2004) looked at the effects of an extra pulse of aviation induced  
23 NO<sub>x</sub> at four months representing the seasonal cycle. Their results showed a seasonal  
24 dependence in the O<sub>3</sub> radiative forcing with a long term net radiative forcing of approximately  
25 zero. Wild et al. (2012) examined the impact of solar flux variations while Shine et al. (2005)  
26 and Berntsen et al. (2005) investigated the effects of atmospheric mixing. However, as reported  
27 in Holmes et al. (2011), model-based estimates of aviation NO<sub>x</sub>-induced changes in O<sub>3</sub> vary by  
28 up to 100%, largely because of differences between models in the ratios of NO : NO<sub>2</sub> and OH :  
29 HO<sub>2</sub>, background NO<sub>x</sub> levels, location and time of emissions, the amount of sunlight, and in  
30 atmospheric mixing (Holmes et al., 2011). Recent studies by Olsen et al. (2013) and Brasseur et

1 al. (2013) found considerable differences between a set of climate-chemistry models (CCMs)  
2 and chemistry transport models (CTMs) in comparisons of the background atmosphere and  
3 aviation NO<sub>x</sub>-induced changes in ozone.

4 In this study, we examine the effect of aviation NO<sub>x</sub> emissions on the atmospheric  
5 concentration of O<sub>3</sub> and hydrogen oxide radicals (HO<sub>x</sub>=OH+HO<sub>2</sub>) and the reduction of CH<sub>4</sub>  
6 lifetime using the latest versions of the atmospheric components of the Community Earth  
7 System Model (CESM) model, namely the Community Atmosphere Model with Chemistry,  
8 Version 4 (CAM4) and Version 5 (CAM5). We further calculate the radiative forcing  
9 associated with the changes in O<sub>3</sub> concentration using the University of Illinois Radiative  
10 Transfer Model (UIUC RTM). While the calculated effects in CAM4 and CAM5 provide a new  
11 reference for the aviation NO<sub>x</sub>-induced effects in comprehensive climate-chemistry models,  
12 they also provide a measure for the effects of different oxidative capacity in the models, due to  
13 differences in description of the physical processes in the model, and especially due to the  
14 different treatment of aerosol processes (see model description).

15 This paper is organized as follows. The following section provides model description. Section 3  
16 discusses the emissions and simulation setup. Section 4 presents the results and section 5  
17 provides the concluding material.

## 18 **2 Model Description**

19 CAM4 and CAM5 (Community Atmosphere Model versions 4 and 5) are the atmospheric  
20 component models for the Community Earth System Model (CESM)  
21 (<http://www.cesm.ucar.edu/>). The details of the physics parameterizations in the CAM4 and  
22 CAM5 models have been discussed extensively in other studies before (e.g. Neale et al., 2011;  
23 Gent et al., 2011; Lamarque et al., 2012). Briefly, CAM5 has been substantially modified in the  
24 representation of physical processes compared to CAM4, including a new shallow convection  
25 scheme, and updated planetary boundary layer (PBL) schemes, revised cloud macrophysics  
26 scheme, updated radiation scheme (Medeiros et al., 2012). These updates improve the  
27 representation of cloud properties and permit assessing the indirect effect of aerosols on clouds,  
28 which is not included in CAM4.

1 Cloud microphysical processes are represented by a prognostic, two-moment formulation for  
2 cloud droplets and cloud ice. Mass and number concentrations of cloud droplets and cloud ice  
3 follow the Morrison and Gettelman (2008) parameterization. The gamma function is employed  
4 to determine liquid and ice particle sizes (Gettelman et al., 2008). The evolution of liquid and  
5 ice particles in time is affected by grid-scale advection, convective detrainment, and turbulent  
6 diffusion. Activation of cloud droplets is a function of aerosol size distribution, aerosol  
7 chemistry, temperature, and vertical velocity (Neale et al., 2011). The cloud macrophysics  
8 scheme imposes full consistency between cloud fraction and cloud condensate. Liquid cloud  
9 fraction is based on a triangular distribution of total relative humidity. Ice cloud fraction is  
10 based on Gettelman et al. (2010) that allows supersaturation via a modified relative humidity  
11 over ice and the inclusion of the ice condensate amount. The aerosol-cloud scheme simulates  
12 full aerosol-cloud interactions such as cloud droplet activation by aerosols, precipitation  
13 processes due to particle size dependence, and explicit radiative interaction of cloud particles  
14 (Liu et al., 2012). Further, CAM5 was successfully coupled to the full chemical mechanism and  
15 released in CESM 1\_2\_0 and versions thereafter (as discussed in detail in Tilmes et al., in  
16 preparation). Since the coupling of aerosols and chemistry in CAM5 has not been released at  
17 the time model runs were performed, a development version of close to CESM1\_2\_0 release  
18 version (cesm1\_2\_beta08\_chem) was used for CAM5 simulations, which includes this  
19 coupling. The CESM1\_0\_3 released version was used for CAM4 simulations. Both models use  
20 the same gas-phase chemical mechanisms including tropospheric and stratospheric chemistry  
21 with about 133 species and 330 photochemical reactions (Lamarque et al., 2012). A complete  
22 list of species and reactions can be found in Lamarque et al. (2012). While the two models use  
23 the same gas-phase chemistry, there are differences in aerosol properties, due to the different  
24 aerosol treatment in CAM4 and CAM5. CAM4 uses a bulk aerosol module with one lognormal  
25 distribution for all aerosols (Lamarque et al., 2012) while CAM5 uses the modal aerosol  
26 module (MAM) (Liu et al., 2012). MAM was developed with two versions, one with seven  
27 lognormal modes (MAM7) and one with three lognormal modes (MAM3) (Liu et al., 2012).  
28 Here, we use the more complete version with seven lognormal modes. MAM7 represents  
29 Aitken, accumulation, primary carbon, fine dust and sea salt, and course dust and sea salt  
30 modes. Within each mode, the mass mixing ratios of the respected aerosols and their number

1 mixing ratios are calculated (Liu et al., 2012). MAM simulates both internal and external  
2 mixing of aerosols, chemical and optical properties of aerosols, and various complicated  
3 aerosols processes (Liu et al., 2012).

4 The UIUC RTM was used offline to calculate the forcing associated with aviation NO<sub>x</sub>-  
5 induced short-term O<sub>3</sub>. Earlier versions of the UIUC RTM have been used in previous research  
6 (e.g., Jain et al., 2000; Naik et al., 2000; Youn et al., 2009; Patten et al., 2011). The UIUC  
7 RTM calculates the flux of solar and terrestrial radiation across the tropopause. The solar  
8 model includes 18 spectral bins from 0.2 to 0.5 microns and includes absorption by H<sub>2</sub>O, O<sub>3</sub>,  
9 O<sub>2</sub>, CO<sub>2</sub>, clouds, and the surface. Scattering processes by clouds, gas-phase molecules, and the  
10 surface are included as well. The terrestrial radiation calculation uses a narrow band model of  
11 absorptivity and emissivity that covers wave numbers from 0 to 3000 cm<sup>-1</sup> at a resolution of 10  
12 cm<sup>-1</sup> for H<sub>2</sub>O, CFC-11, and CFC-12, and of 5 cm<sup>-1</sup> for all other gases. The infrared absorption  
13 parameters for gases are obtained from the HITRAN 2004 database (Rothman et al., 2005).  
14 Surface albedo and emissivity are based on observations, while clouds are based on the  
15 International Satellite Cloud Climatology Project. The use of the same cloud fields for both  
16 CAM4 and CAM5 simulations in the offline radiative forcing calculations ensures that the  
17 differences in the calculated change in radiative forcing are due to the differences in chemistry  
18 and not due to the differences in cloud fields. A previous study by Conley et al. 2013 shows  
19 that using different cloud fields in an offline radiative transfer model makes very little to no  
20 difference in the calculated change of radiative forcing for radiative active species.

### 21 **3 Aviation NO<sub>x</sub> Emissions and Simulation Setup**

22 Both models were run at a horizontal resolution of 1.9° latitude x 2.5° longitude and were  
23 configured with 56 vertical levels covering from the surface up to ~2 hPa with near tropopause  
24 resolution of about 1.3 km. To reduce year-to-year climate variability in the model simulations  
25 and to help detect the aviation NO<sub>x</sub> signal, specified dynamics (“off-line” mode) simulations  
26 were performed. In these simulations, changes in the chemical constituents do not affect the  
27 dynamics. The models used the GEOS DAS v5.1 meteorology for the year 2005 (Rienecker et  
28 al. 2008) which was the closest available assimilated meteorology data to the year of interest  
29 (2006). The aviation emissions for 2006 are from the AEDT aviation emissions analyses

1 (Wilkerson et al., 2010; Olsen et al, 2012). The background emissions of non-aviation short-  
2 lived species (e.g., NO<sub>x</sub>, volatile organic compounds (VOCs)) were obtained from the IPCC  
3 RCP4.5 scenario for year 2005 (van Vuuren et al., 2011) and both models were run with the  
4 same total lighting NO<sub>x</sub> values. The monthly surface concentrations of longer-lived species,  
5 e.g., CO<sub>2</sub>, CH<sub>4</sub>, chlorofluorocarbons (CFCs), and nitrous oxide (N<sub>2</sub>O), were specified as  
6 boundary conditions based on the IPCC RCP4.5 scenario. To analyze the effect of aviation  
7 NO<sub>x</sub> emissions on the background atmosphere, two simulations are performed in each model.  
8 One simulation considers all NO<sub>x</sub> emissions including aviation NO<sub>x</sub>, and the other simulation  
9 has all NO<sub>x</sub> emissions but no aviation NO<sub>x</sub> (control run). The difference between these two  
10 simulations corresponds to the changes induced by aviation NO<sub>x</sub>. The simulations were run for  
11 7 years, cycling through the 2005 meteorology, to reach steady-state with data from the 7<sup>th</sup> year  
12 used in this analysis.

13 Since both models were run with same emissions, same total lighting NO<sub>x</sub> values, and with  
14 identical meteorological fields with 100% nudging, the differences in the description of  
15 aerosols very likely have the largest impact on the chemistry of aviation NO<sub>x</sub>-induced effects,  
16 while differences in clouds may also contribute to some degree. In particular, differences in the  
17 aerosol burden, but especially in the surface area density, that are caused by differences in the  
18 aerosol size distribution (effective radius) and mass, have an influence on the heterogeneous  
19 chemistry and therefore influence the oxidative capacity of the atmosphere and therefore the  
20 chemical composition, as further discussed in Section 4.4. The impact of differences in  
21 dynamics is expected to be small, since in both models the horizontal winds, surface fluxes and  
22 temperatures were prescribed with GEOS meteorological analysis fields.

## 23 **4 Results and Discussions**

### 24 **4.1 Chemistry Diagnosis**

25 Previous intercomparisons of multiple climate-chemistry models indicated that CAM  
26 reasonably simulates the effects of aviation NO<sub>x</sub>-induced emissions on distribution of  
27 tropospheric O<sub>3</sub> and NO<sub>x</sub> (Weber, 2011 and Olsen et al., 2013). However, due to the radiative  
28 importance of ozone in troposphere and stratosphere and in relation to differences in aerosols

1 treatment between the two model configurations used in this study, simulated ozone in the  
2 control runs at representative altitudes is evaluated using an ozonesonde climatology (Tilmes et  
3 al., 2012). This climatology includes observations for the years 1995-2011 and covers averaged  
4 ozone profiles for 41 different ozonesonde stations that are grouped into 12 regions. For our  
5 comparisons, we evaluate ozone at four pressure levels covering the troposphere and lower  
6 stratosphere (50, 250, 500, and 900 hPa) over the 12 areas, which are grouped into three larger  
7 regions (Tropics, Mid-Latitudes, and High Latitudes), as shown in Figure 1. Model results are  
8 interpolated horizontally to all the stations within each region, and averaged over each region.  
9 The comparison between model and observations is illustrated in Taylor-like diagrams for each  
10 of the corresponding pressure levels and regions. A slightly different version of CAM4  
11 including chemistry has been previously tested against ozone observations as well as the  
12 observations of other major atmospheric compounds (e.g., Lamarque et al., 2012).

13 The two model versions are in good agreement at 50 hPa and agree within 10% with the  
14 observed values for the mid- and high latitudes, which is the range of the uncertainty of the  
15 observations, besides for Japan (deviations to observations are around 15%) and for the SH  
16 Polar region for CAM4. The seasonal cycle is well reproduced. The models overestimate the  
17 observed ozone concentration in the Tropics by 25 to 50%, with a poor description of the  
18 seasonal cycle, especially for CAM5.

19 At 250 hPa, both models reproduce high latitude ozone observations within 25% and show a  
20 reasonable agreement with the seasonal cycle. In the Tropics and mid-latitudes, the model  
21 largely overestimates ozone, especially for Japan and the SH and most of the tropical stations.  
22 The overestimate of ozone in the mid-latitudes and tropics in CAM4 was also found in  
23 Lamarque et al. (2012), who noted that this result is an indication of a model estimated  
24 tropopause that is lower than observed and possibly too much transport of ozone into the  
25 troposphere.

26 Of the four pressure levels studied, the models most accurately simulate ozone at the 500 hPa  
27 level. The absolute difference in generated ozone is within 11.7% for both models, which is  
28 within the variability of the observations. CAM4 slightly overestimates ozone at all but one  
29 location. Overall, CAM5 appears to perform better than CAM4 due to a lower percent



1 difference in ozone (6.0% in CAM5 compared to 11.7% in CAM4). The seasonal cycle is  
2 simulated reasonably well for both models, with a correlation coefficient of 0.80 for CAM5 and  
3 0.82 for CAM4.

4 On average, both models perform well in the boundary layer (900 hPa), although there are  
5 several outliers. Both models overestimate the ozone concentration in the Western Europe and  
6 Canada regions. On the other hand, both models underestimate ozone in the SH Mid-Latitude  
7 and SH Polar regions. At all other locations, ozone agrees well with observations. The relative  
8 bias is lower in CAM5 (10.0% compared to 15.7% in CAM4), indicating a better representation  
9 of ozone by CAM5. Additionally, with the exception of the Equatorial Americas region in  
10 CAM4 and the Japan region for both models, the seasonal correlation is excellent (0.81 in both  
11 CAM5 and CAM4).

12 Overall, both models simulate ozone more accurately in the troposphere than in the UTLS and  
13 stratosphere and overestimate ozone in the tropical transition layer. The simulated seasonal  
14 cycle in CAM4 is slightly better than in CAM5 in comparison to observations.

15 Comparisons of O<sub>3</sub>, NO<sub>x</sub>, HNO<sub>3</sub>, PAN, as well as CO to aircraft observations between 2-7 km  
16 (Emmons et al., 2000; Tilmes et al., in preparation), where the majority of the observations  
17 were taken is also shown in Figure 2, both the control and perturbed simulations.

18 In comparison to aircraft data, ozone is slightly overestimated in the tropics, especially for the  
19 perturbed simulations, in agreement with ozonesonde observations, while there is reasonable  
20 agreement in mid- and high latitudes. Both model versions simulate the regional differences in  
21 NO<sub>x</sub> in comparison to available aircraft observations reasonably well, but NO<sub>x</sub> is slightly  
22 underestimated by all model simulations is summer in NH mid-latitudes. Both model versions  
23 overestimate PAN and HNO<sub>3</sub> in tropics and mid-latitudes and high latitude in spring. Model  
24 differences between CAM4 and CAM5 are within the variability of the observations. CO is  
25 underestimated in both model versions, with much larger deviations from the observations for  
26 CAM5 than CAM4. This points to a significant overestimation of OH in CAM5, as also  
27 indicated by the smaller methane lifetime in CAM5 compared to CAM4. The increase in NO<sub>x</sub>  
28 due to aircraft emissions does not affect NO<sub>x</sub>, NO<sub>y</sub>, and CO very much in the altitude

1 considered. However, ozone is slightly increased in the perturbed case for both CAM4 and  
 2 CAM5.

### 3 **4.2 Spatial distribution of NOx emissions**

4 The AEDT NOx emission data used as the input to the model runs had an hourly temporal  
 5 resolution. The spatial distribution of aviation NOx emissions for 2006 is shown in Figure 3  
 6 which amounts to 2.7 Tg (NO<sub>2</sub>)/yr. As in Figure 3, the largest intensity of NOx emissions is in  
 7 the eastern United States, eastern Asia, and Europe. The local maximum in the eastern U.S.  
 8 contributes approximately 0.0136 Tg to the global emissions of NO<sub>2</sub> while the local maximum  
 9 in Europe contributes 0.0154 Tg. Additionally, the peak value in Asia contributes 0.0123 Tg to  
 10 the global total. These values represent the maximum emissions from a single grid cell. The  
 11 main source of NOx emissions occur between 30° and 60°N latitude.

12 Figure 4 shows the seasonal distribution of aviation NOx emissions from 2006. As shown in  
 13 Figure 4, aviation NOx emissions have a different seasonal distribution with the highest amount  
 14 of emissions released in the summer, due to increased air traffic in those months.

### 15 **4.3 Ozone production and loss**

16 Figure 5 shows the aviation NOx-induced annual vertical profile of short-term O<sub>3</sub> production  
 17 and loss as calculated by CAM5 (red) and CAM4 (blue). Both models show the maximum rate  
 18 of ozone production peaking in the upper troposphere/lower stratosphere (UTLS) region where  
 19 the greatest amount of aircraft induced NOx emissions occur.

20 As we analyze the results from the model runs, we use the following chemical reactions for  
 21 ozone production in the troposphere (Sillman, 2012):

22

P1	$VOC + OH \xrightarrow{O_2} RO_2 + H_2O$
P2	$CO + OH \xrightarrow{O_2} HO_2 + CO_2$
P3	$RO_2 + NO \xrightarrow{O_2} secondary\ VOC + HO_2 + NO_2$
P4	$HO_2 + NO \rightarrow OH + NO_2$

P5	$NO_2 + hv \rightarrow NO + O$
P6	$O + O_2 + M \rightarrow O_3 + M$

Ozone destruction in the troposphere, on the other hand, is given by the following reactions (Sillman, 2012):

L1	$NO + O_3 \rightarrow NO_2 + O_2$
L2	$O_3 + hv \xrightarrow{H_2O} 2OH + O_2$
L3	$HCHO + hv \xrightarrow{2O_2} 2HO_2 + CO$
L4	$HO_2 + HO_2 \rightarrow H_2O_2 + O_2$
L5	$RO_2 + HO_2 \rightarrow ROOH + O_2$
L6	$OH + NO_2 \rightarrow HNO_3$

The impact of aviation induced NO<sub>x</sub> on ozone results in a net increase in the rate of ozone production with a maximum around 250hPa, and a net decrease in the rate of ozone production ozone below 450 hPa. Within the UTLS region, the rate of ozone loss decreases due to the increase in HO<sub>2</sub> (Figure 9, as discussed below) reacting with NO (as in equation P4). This process creates NO<sub>2</sub> which further increases O<sub>3</sub> production (by equations P5 and P6). Part of the excess ozone that is created in the UTLS region is transported to lower altitudes. As shown in Figure 5, the rate of ozone loss peaks around 500 hPa. As described by equation L2, at this altitude, excess ozone transported from the UTLS region in the presence of water vapor reacts to form HO<sub>x</sub>, increasing ozone loss. Additional reductions in the net O<sub>3</sub> production are caused by the increased reaction of HO<sub>x</sub> with NO<sub>x</sub> near the surface, resulting in the conversion of NO<sub>x</sub> to HNO<sub>3</sub> (equation L6).

While the patterns of the changes in the simulated ozone production and loss agree well between the models and with previous studies (Köhler et al., 2008), there are differences between CAM4 and CAM5 in the magnitudes. Compared to CAM4, overall ozone production and loss are larger in CAM5, due to the differences in OH between the models. The net rate of ozone production in CAM5 is higher at cruise altitudes and slightly lower at lower altitudes.

1 The maximum net production of ozone is  $1.1 \times 10^{20}$  molecules. $s^{-1}.$ Pa $^{-1}$  in CAM5 and  $1.0 \times 10^{20}$   
2 molecules. $s^{-1}.$ Pa $^{-1}$  in CAM4. CAM4 estimates a maximum rate of production at  $1.2 \times 10^{20}$   
3 molecules. $s^{-1}.$ Pa $^{-1}$  while CAM5 estimates a rate of  $1.4 \times 10^{20}$  molecules. $s^{-1}.$ Pa $^{-1}$ . At lower  
4 altitudes, CAM5 gives a greater rate of ozone loss than CAM4. Both models show a peak in the  
5 ozone loss rate around 600 hPa with values of about  $0.5 \times 10^{20}$  molecules. $s^{-1}.$ Pa $^{-1}$  in CAM5, and  
6 about  $0.4 \times 10^{20}$  molecules. $s^{-1}.$ Pa $^{-1}$  in CAM4. Overall, as found in Figure 1 (as confirmed  
7 through comparisons with ozonesonde data) and shown in Figure 5, CAM5 is more efficient in  
8 producing ozone than CAM4 in most of the atmosphere.

#### 9 **4.4 Global burdens**

10 Table 1 compares the annual mean tropospheric burden of HO<sub>x</sub>, NO<sub>x</sub>, gaseous NO<sub>y</sub> and the  
11 ratios of OH : HO<sub>2</sub> and NO<sub>x</sub> : NO<sub>y</sub> in both CAM4 and CAM5 for both the control run and  
12 aviation NO<sub>x</sub>-perturbed run. The comparison of the burdens presented in Table 1 indicates that  
13 the background atmosphere is relatively different between the two models (e.g. ~8.1%  
14 difference in the background O<sub>3</sub>). While such differences seem to be smaller compared to the  
15 intermodel uncertainty ( $\pm 25\%$ ) reported in Stevenson et al. (2006), there is about 11.8%  
16 difference in the aviation NO<sub>x</sub>-induced annual mean tropospheric O<sub>3</sub> response.

17 As shown in Table 1, The ratio of NO<sub>x</sub> : NO<sub>y</sub> is about 7% higher in CAM5 perturbed run than  
18 in CAM4 perturbed run implying a smaller shift of the NO<sub>x</sub> : NO<sub>y</sub> relationship to NO<sub>y</sub> in  
19 CAM5. The smaller shift of the NO<sub>x</sub> : NO<sub>y</sub> relationship to NO<sub>y</sub> in CAM5 is tied to  
20 heterogeneous reactions and related to less aerosol surface area density in CAM5 compared to  
21 CAM4. Under lower aerosol surface area density, heterogeneous reaction can be less effective  
22 in moving NO<sub>x</sub> to NO<sub>y</sub> and this results in more OH, and shorter CH<sub>4</sub> lifetime (as seen in Table  
23 2). Heterogeneous reactions that are included in CAM chemical mechanism are listed in Eq 1-3.



1 As such, due to less efficient transfer of NO<sub>x</sub> to NO<sub>y</sub> in CAM5 compared to CAM4 there is  
2 more nitrogen available in its reactive form (NO<sub>x</sub>) to trigger the ozone formation reactions in  
3 CAM5, resulting in higher aviation NO<sub>x</sub>-induced ozone perturbation.

#### 4 **4.5 Ozone**

5 The NO<sub>x</sub>-induced changes in tropospheric ozone are complicated by two stages, a short-term  
6 increase in O<sub>3</sub> concentrations associated with a positive forcing, and a long-term reduction of  
7 O<sub>3</sub> concentrations tied to the aviation induced methane decrease. This long term-reduction is  
8 associated with negative forcing (Wild et al., 2001; Stevenson et al., 2004). Since our  
9 simulations were performed with fixed CH<sub>4</sub> mixing ratios at the boundary layer, the calculated  
10 changes in O<sub>3</sub> concentration are the short-term changes.

11 The aviation NO<sub>x</sub>-induced ozone perturbation is shown in Figure 6. Model results from CAM5  
12 are shown on the top panel while CAM4 is on the bottom. The left column shows the mean  
13 zonal ozone perturbation for January, while the right column shows July. As shown in Figure 6,  
14 CAM5 produces a greater amount and wider distribution of ozone in the UTLS region for both  
15 months. The pattern and the localized maximum of the ozone perturbation at 200 hPa in the NH  
16 are about the same in both CAM4 and CAM5. The tropospheric mean change in O<sub>3</sub> is higher in  
17 CAM5 than CAM4 for both January and July. In July, CAM5 generates a tropospheric mean  
18 ozone perturbation of 1.16 ppb (compared to 1.0 in CAM4). In January, CAM5 generates a  
19 tropospheric mean ozone perturbation of 1.18 ppb (compared to 1.1 in CAM4). Overall,  
20 aviation NO<sub>x</sub> emissions from the year 2006 yield an annual tropospheric mean O<sub>3</sub> perturbation  
21 of 1.2 ppb (2.4%) in CAM5 and 1.0 ppb (1.9%) in CAM4. The annual mean O<sub>3</sub> perturbation  
22 peaks at 8.2 ppb (6.4%) in CAM5 and 8.8 ppb (5.2%) in CAM4. Despite the greater production  
23 of annual mean O<sub>3</sub> in CAM5, the peak is slightly lower in CAM5 compared to CAM4, since  
24 the produced O<sub>3</sub> is more distributed towards the surface in CAM5.

25 As shown in Figure 6, the UTLS ozone perturbation is much greater in July than in January for  
26 both models. This is due to differences in the length of daylight between those months,  
27 increased photochemistry, and higher aviation NO<sub>x</sub> emissions in July (as shown in Figure 4).  
28 The increased daylight allows more photolysis of NO<sub>2</sub> to occur, which generates O<sub>3</sub> (equations

1 P5 and P6). Also note the differences in ozone perturbations in the lower troposphere between  
2 January and July. In the summer, the ozone perturbation at lower altitudes is weaker due to  
3 greater surface deposition and also the shorter photochemical lifetime of ozone through  
4 increased water vapor (and more HOx giving increased ozone loss) (Hodnebrog et al., 2011).  
5 Additionally, both models show the maximum ozone impact increasing towards high latitudes  
6 in the NH in July. A similar result was found by Hoor et al. (2009) who showed a maximum  
7 zonal mean ozone perturbation centered around 75° N during June.

8 As shown in both months and models, a mid-latitude perturbation extends from 400 hPa  
9 down towards the surface. This feature agrees with past studies by Hoor et al. (2009), Koffi et  
10 al. (2010), and Hodnebrog et al. (2011). Hoor et al. (2009) notes that this feature is due to more  
11 vigorous boundary layer mixing and convective transport into the free troposphere during the  
12 summer.

13 As shown in Figure 7, annual mean column ozone changes are relatively zonally well mixed,  
14 however, several ‘hotspots’ in both CAM5 and CAM4 exist just north of the Mediterranean and  
15 off the western coast of Europe. A more uniform spread is seen over Europe, the western half  
16 of Asia, the Atlantic Ocean and a small strip at about 45°N in the Pacific Ocean. These  
17 ‘hotspots’ are stronger in CAM5 and peak at about 2.3 DU compared to 2.1 DU in CAM4. As  
18 expected, the ozone impact is very small in the SH. A sharp ozone gradient exists in the NH  
19 subtropics, as was also seen in previous studies. The ozone concentration continues to increase,  
20 with the maximum values between 30 and 60° N. Hoor et al. (2009) and Hodnebrog et al.  
21 (2011) found a similar distribution. Overall, aviation NOx emissions from the year 2006 lead to  
22 a 1.0 and 0.9 DU change in annual global mean ozone column in CAM5 and CAM4,  
23 respectively.

#### 24 **4.6 HOx**

25 The hydroxyl radical (OH) plays an important role in the creation of atmospheric ozone. It is  
26 the primary oxidizing agent of the troposphere, removing greenhouse gases such as CH<sub>4</sub>, CO,  
27 HCFCs, and others. Production of OH by O<sub>3</sub> is given by equation L2. Figure 8 shows the  
28 increase in aviation induced zonal mean annual OH perturbations.

1 Similar to ozone, the impact of aviation emitted NO<sub>x</sub> on tropospheric OH production is largest  
2 in July. This increase in OH during the summer months is also due to the enhanced  
3 photochemistry. Aircraft emissions have the largest zonal mean ozone impact in the UTLS  
4 region in mid- and high latitudes in the NH between 40-90°N. However, the OH perturbation is  
5 more concentrated south of the O<sub>3</sub> perturbations. The more southern position of OH is due to  
6 the increased humidity and the lower solar zenith angle, which are essential to produce the  
7 excited oxygen atom (O(<sup>1</sup>D)) and hence higher OH concentrations. This result agrees well with  
8 recent studies by Hoor et al. (2009) and Hodnebrog et al. (2011). Additionally, there is a greater  
9 perturbation of OH extending towards the surface over mid-latitudes than there was of O<sub>3</sub>. This  
10 is due to the increased production of HO<sub>x</sub> in the mid-troposphere triggered by O<sub>3</sub> photolysis and  
11 the presence of water vapor. Additionally, both models show OH perturbations extending from  
12 400 hPa down to the surface above 40°N. This feature is much weaker in January because the  
13 UV actinic flux necessary for OH production is much smaller in the NH.

14 Between the two models, the OH concentration is higher in CAM5 than CAM4. This is a result  
15 of higher O<sub>3</sub> production in CAM5. In July, the CAM5 aviation NO<sub>x</sub>-induced tropospheric  
16 mean OH perturbation is  $1.2 \times 10^4$  molecules.cm<sup>-3</sup> (compared to  $9.1 \times 10^3$  in CAM4). In January,  
17 the CAM5 aviation NO<sub>x</sub>-induced tropospheric mean OH perturbation is  $9.4 \times 10^3$  molecules cm<sup>-3</sup>  
18 (compared to  $6.4 \times 10^3$  in CAM4). Overall, aviation NO<sub>x</sub> emissions from the year 2006 lead to  
19 an annual tropospheric mean OH perturbation of  $1.1 \times 10^4$  molecules.cm<sup>-3</sup> in CAM5 and  $7.8 \times 10^3$   
20 molecules.cm<sup>-3</sup> in CAM4.

21 Figure 9 shows the CAM4 and CAM5 HO<sub>2</sub> perturbations due to aviation NO<sub>x</sub> emissions.  
22 Areas that experience an increase in HO<sub>2</sub> concentrations are shown in red and areas that  
23 experience a decrease in HO<sub>2</sub> are in blue. Increases in NO<sub>x</sub> emissions from aviation increases  
24 OH levels by shifting the HO<sub>x</sub> balance in favor of OH production, given by equation P4  
25 (Stevenson et al., 2004; Berntsen et al., 2005; Köhler et al., 2008). This process results in HO<sub>2</sub>  
26 loss at cruise altitudes. As expected, the areas of HO<sub>2</sub> loss correspond to the areas that  
27 experienced an increase in OH concentrations.

28 In January, there is a greater rate of HO<sub>2</sub> consumption in the UTLS region in CAM5 than there  
29 is in CAM4 due to higher OH production. Following equation P4, this HO<sub>2</sub> reacts with aircraft

1 emitted NO to give OH and NO<sub>2</sub>. Similarly, the rate of HO<sub>2</sub> consumption is also greater in the  
2 UTLS region during July in CAM5 as well. When comparing Figure 9 with Figure 8, the  
3 locations of maximum HO<sub>2</sub> loss correspond with the locations of maximum OH concentration  
4 changes, indicating that reaction P4 is a significant reaction in OH production in the UTLS  
5 region. At lower altitudes in July, the transported ozone is photolyzed in the presence of water  
6 vapor, thus increasing OH, and subsequently HO<sub>2</sub>.

#### 7 **4.7 CH<sub>4</sub>**

8 The hydroxyl radical OH is the largest sink of CH<sub>4</sub> in the atmosphere. As the OH concentration  
9 is effected by aircraft emissions, so is the methane concentration and its lifetime.

10 Figure 10 shows the aviation induced annual zonal averaged CH<sub>4</sub> loss rate for CAM5 (left) and  
11 CAM4 (right). In both CAM5 and CAM4, the change in methane loss is mostly confined to the  
12 NH at a location south of the OH perturbation (between 0-30°N). This predominately occurs  
13 due to the increase in the methane-OH reaction rate constant with higher temperatures at lower  
14 altitudes. As such, in both models the position of the maximum CH<sub>4</sub> loss is below the cruise  
15 altitude. As shown in Figure 10, the CH<sub>4</sub> loss is higher in CAM5 than CAM4 due to the higher  
16 production of aviation induced OH in CAM5. Table 2 shows the reduction in methane lifetimes  
17 as calculated for both CAM4 and CAM5.

18 Table 2 shows the global annual average CH<sub>4</sub> lifetimes against reaction with OH, as calculated  
19 by CAM4 and CAM5 for the background (control) run and the NO<sub>x</sub>-perturbed run. It is noted  
20 that same as most other models (Voulgarakis et al., 2013 and Naik et al., 2013) the calculated  
21 lifetimes here are shorter than the CH<sub>4</sub> lifetime derived based on Methyl chloroform analysis  
22 (Prather et al., 2012). The change in CH<sub>4</sub> lifetime is also presented as the percent change in  
23 lifetime. The reduction in CH<sub>4</sub> lifetime calculated in CAM5 and CAM4 is 1.69%  
24 (2.50%/ [TgN/yr]) and 1.40% (1.71%/ [TgN/yr]), respectively, excluding the feedback of  
25 changes in methane concentration on its own lifetime (e.g. Prather 1994; Fuglestedt et al.  
26 1999; Wild et al. 2001 and IPCC 2007). The CAM4 reduction in CH<sub>4</sub> lifetime falls within the -  
27 1.4±0.4 (%/[TgN/yr]) to -1.6±0.37 (%/[TgN/yr]) range reported by Hodnebrog et al. (2011).  
28 The CAM5 simulated change in CH<sub>4</sub> lifetime is greater than the upper range reported by



1 Hodnebrog et al. (2011). Inclusion of the aviation induced methane feedback on its lifetime  
2 further decreases the lifetime by a factor of 1.4 (IPCC, 2001). The greater reduction of the CH<sub>4</sub>  
3 lifetime in CAM5 is the result of a greater increase in the aviation induced OH concentration in  
4 CAM5.

#### 5 **4.8 Aviation NO<sub>x</sub>-Induced Ozone Radiative Forcings**

6 The aviation NO<sub>x</sub>-induced short-term O<sub>3</sub> RFs were calculated as the difference of the radiation  
7 imbalance between the NO<sub>x</sub>-perturbed and control simulations at the tropopause calculated  
8 with the UIUC RTM, excluding the effects of stratospheric adjustment. Figure 11 shows the  
9 yearly averaged short-term ozone RF for CAM5 (left) and CAM4 (right). Both models show  
10 the greatest RF in the NH between 30-60°N with highest RF changes over Southern Europe and  
11 the Middle East. As expected, the O<sub>3</sub> RF from aviation is low in the SH. The greatest RF values  
12 in the SH are over the SH tropical Pacific Ocean and are most likely due to air traffic between  
13 Australia and the United States. Interestingly, radiative forcing values over Asia are relatively  
14 low, given the amount of NO<sub>x</sub> emissions from this area. Additionally, it appears that the  
15 maximum radiative forcing from Europe's emissions has shifted to the Mediterranean,  
16 indicating that these aircraft emissions have a maximum impact downwind of the source. These  
17 results agree well with Hodnebrog et al. (2011).

18 The associated global mean short-term ozone RF is 40.3 and 36.5 mWm<sup>-2</sup> in CAM5 and  
19 CAM4, respectively. CAM5 has a greater annual ozone RF, due to the greater ozone  
20 perturbation, which largely accounts for the differences in radiative forcings. It is noted that  
21 Fuglestvedt et al. 2008 compares the aviation contribution in changing the radiative forcing to  
22 the contribution from other transportation sectors.

### 23 **5 Conclusion**

24 CAM5 and CAM4 simulate background ozone to within 13% and 18% (on average and at all  
25 the locations), respectively, compared to ozonesonde datasets. Based on the comparison with  
26 ozonesonde observations, CAM5 was more accurate at determining the ozone distribution in  
27 the troposphere and lower stratosphere.

1 Aviation induced O<sub>3</sub> is higher in CAM5 than CAM4 with an annual tropospheric mean O<sub>3</sub>  
2 perturbation of 1.2 ppb (2.4%) in CAM5 and 1.0 ppb (1.9%) in CAM4. In July, CAM5  
3 generates an aviation NO<sub>x</sub>-induced tropospheric mean ozone perturbation of 1.16 ppb  
4 (compared to 1.0 in CAM4) with a corresponding value of 1.18 ppb in Jan (compared to 1.1 in  
5 CAM4).

6 As found in previous studies, the maximum effect from aircraft NO<sub>x</sub> emissions on ozone is in  
7 the NH Upper Troposphere/Lower Stratosphere region. This is due to the high frequency of  
8 subsonic aircraft flying in this region. The aircraft-induced ozone perturbation is greater in the  
9 NH summer due to the enhanced photochemistry. In January, the ozone perturbation mixes  
10 more towards the surface due to the longer photochemical lifetime of ozone and the slower  
11 surface deposition rate than in July.

12 The hydroxyl perturbations are located to the south and at a lower altitude than the position of  
13 the maximum change in ozone. This is due to the lower zenith angle and increased humidity  
14 which are essential to produce the excited oxygen atom (O(<sup>1</sup>D)) and hence higher OH  
15 concentrations. Overall, the aviation NO<sub>x</sub>-induced change in OH is higher in CAM5 in  
16 accordance with higher ozone production. The induced changes in OH concentrations increase  
17 the methane (CH<sub>4</sub>) loss rate and reduce its lifetime by 1.69% and 1.40% in CAM5 and CAM4,  
18 respectively.

19 Results indicate a global mean O<sub>3</sub> RF of 40.3 and 36.5 mWm<sup>-2</sup> in CAM5 and CAM4,  
20 respectively. Both models agree that the maximum O<sub>3</sub> radiative forcing is between 30-60°N.  
21 However, it is interesting to note that it appears that the maximum RF is downwind of a local  
22 maximum NO<sub>x</sub> source.

23 This study is the first evaluation of aviation NO<sub>x</sub> effects in CAM5 which simulates the size  
24 distribution of aerosols, both internal and external mixing of aerosols, chemical and optical  
25 properties of aerosols. It is noted that while the simulated change in ozone is relatively different  
26 between the two models, the difference between CAM4 and CAM5 ozone responses is  
27 considerably smaller than the current estimates of the uncertainty in aviation effects on ozone.  
28 The difference in aviation NO<sub>x</sub>-induced effects between the two models is related to the

1 difference between the two models configuration used in this study (i.e. difference in aerosols  
2 treatment). More detailed analyses are required to explore the impact of the differences in the  
3 representation of the background atmosphere and treatment of aerosols processes on aviation  
4 NO<sub>x</sub>-induced effects to a greater extent.

## 5 **Acknowledgments**

6 The authors would like to thank the Federal Aviation Administration, Aviation Climate Change  
7 Research Initiative (ACCRI) for support under Contract #: 10-C-NE-UI amendment 001 and  
8 The Partnership for AiR Transportation Noise and Emissions Reduction (PARTNER). The  
9 opinions, findings, and conclusions or recommendations expressed in this material are those of  
10 the authors and do not necessarily reflect the views of ACCRI, PARTNER, or the FAA. This  
11 work was partially supported by the U.S. Department of Transportation, the Illinois Department  
12 of Transportation and the Transportation Research and Analysis Computing Center. The  
13 authors would like to thank the National Center for Atmospheric Research (NCAR) for the  
14 support with computing time and NCAR is supported by the National Science Foundation  
15 (NSF). The CESM project (which includes CAM4, CAM5 and CAM-chem) is supported by the  
16 National Science Foundation and the Office of Science (BER) of the U. S. Department of  
17 Energy. The authors would like to also thank Dr. Francis Vitt (NCAR) for his help in  
18 integrating aviation NO<sub>x</sub> emissions into CAM5.

## 19 **References**

20 Arnold, F., Scheid, J., Stilp, T., Schlager, H., and Reinhardt, M. E.: Measurements of jet  
21 aircraft emissions at cruise altitude I: The odd-nitrogen gases NO, NO<sub>2</sub>, HNO<sub>2</sub> and HNO<sub>3</sub>,  
22 Geophysical Research Letters, 19, 2421-2424, 1992.

23  
24 Beck, J. P., Reeves, C. E., De Leeuw, F. A., and Penkett, S. A.: The effect of aircraft emissions  
25 on tropospheric ozone in the northern hemisphere, Atmospheric Environment, Part A. General  
26 Topics, 26, 17-29, 1992.

1 Berntsen, T. K., Fuglestedt, J. S., Joshi, M. M., Shine, K. P., Stuber, N., Ponater, M., Sausen,  
2 R., Hauglustaine, D. A., and Li, L.: Response of climate to regional emissions of ozone  
3 precursors: Sensitivities and warming potentials, *Tellus B*, 57B, 283 – 304, 2005.  
4

5 Borucki, W. J., Whitten, R. C., Watson, V. R., Woodward, H. T., Riegel, C. A., Capone, L. A.,  
6 and Becker, T.: Model predictions of latitude-dependent ozone depletion due to supersonic  
7 transport operations, *AIAA Journal*, 14 =, 1738-1745, 1976.  
8

9 Brasseur, G. P., Müller, J.-F., and Granier, C.: Atmospheric impact of NO<sub>x</sub> emissions by  
10 subsonic aircraft: A three-dimensional model study, *Journal of Geophysical Research*, 101  
11 (D1), 1423–1428, 1996.  
12

13 Brasseur, P. G., Weber, B., Damoah, R., Douglass, A. R., Jacobson, M. Z., Lee, H., Liang, Q.,  
14 Olsen, S. C., Oman, L. D., Ott, L., Pawson, S., Selkirk, H., Sokolov, A., Stolarski, R. S.,  
15 Unger, N., and Wuebbles, D. J.: Model intercomparison of ozone sensitivity to NO<sub>x</sub> emissions  
16 in the vicinity of the extratropical tropopause, *Geophysical Research Letters*, submitted, 2013.  
17

18 Climatic Impact Assessment Program (CIAP), Report of findings, The effects of stratospheric  
19 pollution by aircraft, Rep. DOT-TST-75-50, U.S. Dep. of Transp., Washington, D.C., 1974.  
20

21 Collins, W. J., Bellouin, N., Doutriaux-Boucher, M., Gedney, N., Halloran, P., Hinton, T.,  
22 Hughes, J., Jones, C. D., Joshi, M., Liddicoat, S., Martin, G., O'Connor, F., Rae, J., Senior, C.,  
23 Sitch, S., Totterdell, I., Wiltshire, A., and Woodward, S.: Development and evaluation of an  
24 Earth-system model – HadGEM2, *Geoscientific Model Development Discussion*, 4, 997-1062,  
25 2011.  
26

27 Crutzen, P. J.: SST's: A threat to the Earth's ozone shield, *Ambio*, 1, 1972.  
28

1 Dameris, M., Grewe, V., Köhler, I., Sausen, R., Bruhl, C., Grooss, J. U., and Steil, B.: Impact  
2 of aircraft NO<sub>x</sub> emissions on tropospheric and stratospheric ozone. Part II: 3-D model results,  
3 Atmospheric Environment, 32, 3185–3199, 1998.

4

5 Derwent, R. G.: Two-dimensional model studies of the impact of aircraft exhaust emissions on  
6 tropospheric ozone, Atmospheric Environment, 18, 1997-2007, 1982.

7

8 Derwent, R. G., Collins, W. J., Johnson, C. E., and Stevenson, D. S.: Transient behavior of  
9 tropospheric ozone precursors in a global 3-D CTM and their indirect greenhouse effects,  
10 Climatic Change, 49, 463-487, 2001.

11

12 Emmons, L. K., Walters, S., Hess, P. G., Lamarque, J.-F., Pfister, G. G., Fillmore, D., Granier,  
13 C., Guenther, A., Kinnison, D., Laepple, T., Orlando, J., Tie, X., Tyndall, G., Wiedinmyer, C.,  
14 Baughcum, S. L., and Kloster, S.: Description and evaluation of the Model for OZone And  
15 Related chemical Tracers, version 4 (MOZART-4), Geoscientific Model Development, 3, 43–  
16 67, 2010.

17

18 Fitcher, C., Marquart, S., Sausen, R., and Lee, D. S.: The impact of cruise altitude on contrails  
19 and related radiative forcing, Meteorologische Zeitschrift, 14, 563 – 572, 2005.

20

21 Flatøy, F., and Hov, Ø.: Three-dimensional model studies of the effect of NO<sub>x</sub> emissions from  
22 aircraft on ozone in the upper troposphere over Europe and the North Atlantic, Journal of  
23 Geophysical Research, 101 (D1), 1401-1422, 1996.

24

25 Fuglestvedt, J. S., Berntsen, T., Isaksen, I. S. A., Huiting, M., Liang, X.-Z. , and Wang, W.-C.:  
26 Climatic forcing of nitrogen oxides through changes in tropospheric ozone and methane; global  
27 3D model studies, Atmospheric Environment, 33, 961-977, 1999.

28

1 Fuglestad, J. S., Berntsen T., Myhre G., Rypdal K. and Skeie R. B.: Climate forcing from  
2 the Transport Sectors, Proceedings of the National Academy of Sciences (PNAS), vol 105 (no.  
3 2), 454-458, 2008.

4

5 Gauss, M., Myhre, G., Pitari, G., Prather, M. J., Isaksen, I. S. A., Berntsen, T. K., Brasseur, G.  
6 P., Dentener, F. J., Derwent, R. G., Hauglustaine, D. A., Horowitz, L. W., Jacob, D. J.,  
7 Johnson, M., Law, K. S., Mickley, L. J., Müller, J.-F., Plantevin, P.-H., Pyle, J. A., Rogers, H.  
8 L., Stevenson, D. S., Sundet, J. K., van Weele, M., and Wild, O.: Radiative forcing in the 21st  
9 century due to ozone changes in the troposphere and the lower stratosphere, Journal of  
10 Geophysical Research: Atmospheres, 108 (D9), 2003.

11

12 Gauss, M., Isaksen, I. S. A., Lee, D. S., and Søvde, O. A.: Impact of aircraft NO<sub>x</sub> emissions on  
13 the atmosphere – tradeoffs to reduce the impact, Journal of Atmospheric Chemistry and  
14 Physics, 6, 1529-1548, 2006.

15

16 Gent, P. R., Danabasoglu, G., Donner, L. J., Holland, M. M., Hunke, E. C., Jayne, S. R.,  
17 Lawrence, D. M., Neale, R. B., Rasch, P. J., Vertenstein, M., Worley, P. H., Yang, Z.-L., and  
18 Zhang, M.: The community climate system model version 4, Journal of Climate, 24, 4973-  
19 4991, 2001.

20

21 Gettelman, A., Morrison, H., and Ghan, S. J.: A new two-moment bulk stratiform cloud  
22 microphysics scheme in the NCAR Community Atmosphere Model (CAM3), Part II: Single-  
23 column and global results, Journal of Climate, 21, 3660–3679, 2008.

24

25 Gettelman, A., Liu, X., Ghan, S. J., Morrison, H., Park, S., Conley, A. J., Klein, S. A., Boyle,  
26 J., Mitchell, D. L., and Li, J.-LF.: Global simulations of ice nucleation and ice supersaturation  
27 with an improved cloud scheme in the Community Atmosphere Model, Journal of Geophysical  
28 Research, 115, D18216, doi:10.1029/2009JD013797, 2010.

29

1 Gettelman, A., Liu, X., Barahona, D., Lohmann, U., and Chen, C.: Climate impacts of ice  
2 nucleation, *Journal of Geophysical Research*, 117, D20201, doi:10.1029/2012JD017950, 2012.  
3  
4 Gettelman, A. and Chen, C.: The climate impact of aviation aerosols, *Journal of Geophysical  
5 Research*, 40 (11) (2013), pp. 2785-2789, DOI: 10.1002/grl.50520, 2013.  
6 Hesstvedt, E.: Reduction of stratospheric ozone from high-flying aircraft, studied in a two-  
7 dimensional photochemical model with transport, *Canadian Journal of Chemistry*, 52, 1592-  
8 1598, 1974.  
9  
10 Hodnebrog, Ø., Berntsen, T. K., Dessens, O., Gauss, M., Grewe, V., Isaksen, I. S. A., Koffi, B.,  
11 Myhre, G., Olivié, D., Prather, M. J., Pyle, J. A., Stordal, F., Szopa, S., Tang, Q., Velthoven,  
12 P., Williams, J. E., and Ødemark, K.: Future impact of non-land based traffic emissions on  
13 atmospheric ozone and OH – an optimistic scenario and a possible mitigation strategy, *Journal  
14 of Atmospheric Chemistry and Physics*, 11, 11293–11317, 2011.  
15 Holmes, C. D., Tang, Q., and Prather, M. J.: Uncertainties in climate assessment for the case of  
16 aviation NO, *Proceedings of the National Academy of Sciences, U.S.A.*, 108, 10997–11002,  
17 2011.  
18  
19 Hoor, P., Borcken-Kleefeld, J., Caro, D., Dessens, O., Endresen, O., Gauss, M., Grewe, V.,  
20 Hauglustaine, D., Isaksen, I. S. A., Jöckel, P., Lelieveld, J., Meijer, E., Olivie, D., Prather, M.,  
21 Schnadt Poberaj, C., Staehelin, J., Tang, Q., van Aardenne, J., van Velthoven, P., and Sausen,  
22 R.: The impact of traffic emissions on atmospheric ozone and OH: results from QUANTIFY,  
23 *Journal of Atmospheric Chemistry and Physics*, 9, 3113-3136, 2009.  
24  
25 Horowitz, L. W., Walters, S., Mauzerall, D. L., Emmons, L. K., Rasch, P. J., Granier, C., Tie,  
26 X., Lamarque, J.-F., Schultz, M. G., Tyndall, G. S., Orlando, J. J., and Brasseur, G. P.: A  
27 global simulation of tropospheric ozone and related tracers, Description and evaluation of  
28 MOZART, version 2, *Journal of Geophysical Research*, 108, 4784, 2003.  
29

1 IPCC, 1999: Aviation and the global atmosphere, Intergovernmental Panel on Climate Change.  
2 Penner, J., et al., Eds., Cambridge University Press, Cambridge, UK, 1999.  
3  
4 IPCC, 2001: Climate change, The scientific basis. Contribution of Working Group I to the  
5 Third Assessment Report of the Intergovernmental Panel on Climate Change, Houghton, J. T.,  
6 et al., Eds., Cambridge University Press, Cambridge, UK, 2001.  
7  
8 IPCC, 2007: Climate change, The physical science basis. Contribution of Working Group I to  
9 the Fourth Assessment Report of the Intergovernmental Panel on Climate Change. Solomon, S.,  
10 et al., Eds, Cambridge University Press, Cambridge, UK, 2007.  
11  
12 Penner, J. E., Lister, D. H., Griggs, D. J., Dokken, D. J., McFarland M., (Eds.):  
13 Intergovernmental Panel on Climate Change, Aviation and the Global Atmosphere, Cambridge  
14 University Press, Cambridge, UK, 1999.  
15  
16 Prather, M. J.: Lifetimes and eigenstates in atmospheric chemistry, Journal of Geophysical  
17 Research Letter., 21, 801-4, 1994.  
18  
19 Isaksen, I. S. A., Granier, C., Myhre, G., Berntsen, T. K., Dalsøren, S. B., Gauss, M., Klimont,  
20 Z., Benestad, R., Bousquet, P., Collins, W., Cox, T., Eyring, V., Fowler, D., Fuzzi, S., Jöckel,  
21 P., Laj, P., Lohmann, U., Maione, M., Monks, P., Prevo, A. S. H., Raes, F., Richter, A.,  
22 Rognerud, B., Schulz, M., Shindell, D., Stevenson, D. S., Storelvmo, T., Wang, W.-C., van  
23 Weele, M., and Wuebbles, D.: Atmospheric composition change: climate–chemistry  
24 interactions, Atmospheric Environment, 43, 5138-5192, 2009.  
25  
26 Johnson, C.: Impact of aircraft and surface emissions of nitrogen oxides on tropospheric ozone  
27 and global warming, Nature, 355, 69-71, 1992.  
28



1 Johnson, C. E., Derwent, R. G.: Relative radiative forcing consequences of global emissions of  
2 hydrocarbons, carbon monoxide and NO<sub>x</sub> from human activities estimated with a zonally-  
3 averaged two-dimensional model, *Climatic Change*, 34, 439-462, 1996.

4

5 Johnston, H. S.: Reduction of stratospheric ozone by nitrogen oxide catalysts from supersonic  
6 transport exhaust, *Science*, 173, 517-522, 1971.

7

8 Kinnison, D. E., Brasseur, G. P., Walters, S., Garcia, R. R., Marsh, D. A., Sassi, F., Boville, B.  
9 A., Harvey, L., Randall, C., Emmons, L., Lamarque, J.-F., Hess, P., Orlando, J., Tyndall, G.,  
10 Tie, X. X., Randel, W., Pan, L., Gettelman, A., Granier, C., Diehl, T., Niemeier, U., and  
11 Simmons, A. J.: Sensitivity of chemical tracers to meteorological parameters in the MOZART-  
12 3 chemical transport model, *Journal of Geophysical Research*, 112, D20302,  
13 doi:10.1029/2006JD007879, 2007.

14

15 Kinnison, D. E., Marsh, D. R., Garcia, R. R., Vitt, F., Tilmes, S., Mills, M. J., Lamarque, J.-F.,  
16 Emmons, L. K., Orlando, J. J., Gettelman, A., Liu, H.-L., Yudin, V., Park, M., Randel, W., Pan,  
17 L. L., Brakebusch, M., Randall, C. E., and Hess, P.: Description and evaluation of the Whole  
18 Atmosphere Community Climate Model (WACCM): Chemistry Update, in preparation, 2011.

19

20 Koffi, B., Szopa, S., Cozic, A., Hauglustaine, D., and van Velthoven, P.: Present and future  
21 impact of aircraft, road traffic and shipping emissions on global tropospheric ozone, *Journal of*  
22 *Atmospheric Chemistry and Physics*, 10, 681-711, 2010.

23 Köhler, M. O., Radel, G., Dessens, O., Shine, K. P., Rogers, H. L., Wild, O., and Pyle, J. A.:  
24 Impact of perturbations to nitrogen oxide emissions from global aviation, *Journal of*  
25 *Geophysical Research*, 113, 2008.

26

27 Lamarque, J.-F., Emmons, L. K., Hess, P. G., Kinnison, D. E., Tilmes, V., Vitt, V., Heald, V.,  
28 Holland, E. A., Lauritzen, P. H., Neu, J., Orlando, J. J., Rasch, P., and Tyndall, G.: CAM-chem:  
29 Description and evaluation of interactive atmospheric chemistry in CESM, *Geoscientific Model*  
30 *Development Discussions*, 5, 369 – 411, 2011.

1  
2 Lee, D. S., Fahey, D. W., Forster, P. M., Newton, P. J., Wit, R. C. N., Lim, L. L., Owen, B.,  
3 and Sausen, R.: Aviation and global climate change in the 21<sup>st</sup> century, *Atmospheric*  
4 *Environment*, 43, 3520 – 3537, 2009.  
5  
6 Liang, Q., Rodriguez, J. M., Douglass, A. R., Crawford, J. H., Olson, J. R., Apel, E., Bian, H.,  
7 Blake, D. R., Brune, W., Chin, M., Colarco, P. R., da Silva, A., Diskin, G. S., Duncan, B. N.,  
8 Huey, L. G., Knapp, D. J., Montzka, D. D., Nielsen, J. E., Pawson, S., Riemer, D. D.,  
9 Weinheimer, A. J., and Wisthaler, A.: Reactive nitrogen, ozone and ozone production in the  
10 Arctic troposphere and the impact of stratosphere-troposphere exchange, *Journal of*  
11 *Atmospheric Chemistry and Physics*, 11, 13181-13199, 2011.  
12  
13 Liu, X., Easter, R. C., Ghan, S. J., Zaveri, R., Rasch, P., Shi, X., Lamarque, J.-F., Gettelman,  
14 A., Morrison, H., Vitt, F., Conley, A., Park, S., Neale, R., Hannay, C., Ekman, A., Hess, P.,  
15 Mahowald, N., Collins, W., Iacono, M., Bretherton, C., and Flanner, M.: Toward a minimal  
16 representation of aerosol direct and indirect effects: Model description and evaluation,  
17 *Geoscientific Model Development Discussion*, 4, 3485-3598, doi:10.5194/gmdd-4-3485-2012,  
18 2012.  
19  
20 McElroy, M. B., Wofsy, S. C., Penner, J. E., and McConnell, J. C.: Atmospheric ozone:  
21 Possible impact of stratospheric aviation, *Journal of the Atmospheric Sciences*, 31, 287, 1974.  
22  
23 Meinshausen, M., Raper, S. C. B., and Wigley, T. M. L.: Emulating coupled atmosphere-ocean  
24 and carbon cycle models with a simpler model, *MAGICC6 – Part 1: Model description and*  
25 *calibration*, *Journal of Atmospheric Chemistry and Physics*, 11, 1417–1456, 2011.  
26  
27 Medeiros, B., Williamson, D. L., Hannay, C., and Olson, J. G.: Southeast Pacific stratocumulus  
28 in the Community Atmosphere Model, *Journal of Climate*, 25, 6175–6192, 2012.

1 Morrison, H., and Gettelman, A.: A new two-moment bulk stratiform cloud microphysics  
2 scheme in the NCAR Community Atmosphere Model (CAM3), Part I: Description and  
3 numerical tests, *Journal of Climate*, 21, 3642–3659, 2008.

4

5 Naik, V., Voulgarakis, A., Fiore, A. M., Horowitz, L. W., Lamarque, J.-F., Lin, M., Prather, M.  
6 J., Young, P. J., Bergmann, D., Cameron-Smith, P. J., Cionni, I., Collins, W. J., Dalsøren, S. B.,  
7 Doherty, R., Eyring, V., Faluvegi, G., Folberth, G. A., Josse, B., Lee, Y. H., MacKenzie, I. A.,  
8 Nagashima, T., van Noije, T. P. C., Plummer, D. A., Righi, M., Rumbold, S. T., Skeie, R.,  
9 Shindell, D. T., Stevenson, D. S., Strode, S., Sudo, K., Szopa, S., and Zeng, G.: Preindustrial to  
10 present day changes in tropospheric hydroxyl radical and methane lifetime from the  
11 Atmospheric Chemistry and Climate Model Intercomparison Project (ACCMIP), *Journal of*  
12 *Atmospheric Chemistry and Physics*, 13, 5277-5298, doi:10.5194/acpd-12-30755-2012, 2013.

13

14 Neale, R. B., Richter, J., Park, S., Lauritzen, P. H., Vavrus, S. J., Rasch, P. J., and Zhang, M.:  
15 The mean climate of the Community Atmosphere Model (CAM4) in forced SST and fully  
16 coupled experiments, *Journal of Climate*, 26, 5150-5168, DOI: 10.1175/JCLI-D-12-00236.1,  
17 2013.

18

19 Neu, J. L., and Prather, M. J.: Toward a more physical representation of precipitation  
20 scavenging in global chemistry models: cloud overlap and ice physics and their impact on  
21 tropospheric ozone. *Journal of Atmospheric Chemistry and Physics Discussions*, 11, 24413–  
22 24466, 2011.

23

24 Olsen, S. C., and Wuebbles, D. J.: Comparison of global 3-D aviation emissions datasets,  
25 *Journal of Atmospheric Chemistry and Physics*, 12, 16885 – 16992, 2012.

26

27 Olsen, S. C., Brasseur, G. P., Wuebbles, D. J., Barrett, S., Dang, H., Eastham, S. D., Jacobson,  
28 M. Z., Khodayari, A., Selkirk, H., Sokolov, A., Unger N.: Comparison of model estimates of  
29 the effects of aviation emissions on atmospheric ozone and methane, *Geophysical Research*  
30 *Letters*, accepted, 2013.

1  
2 Patten, K. O., Khamaganov, V. G., Orkin, V. L., Baughcum, S. L., Wuebbles, D. J.: OH  
3 reaction rate constant, IR absorption spectrum, ozone depletion potentials and global warming  
4 potentials of 2-bromo-3,3,3-trifluoropropene, *Journal of Geophysical Research*, 116, D24307.  
5 2011.  
6  
7 Price, C., Penner, J., and Prather, M.: NO<sub>x</sub> from lightning: Global distribution based on  
8 lightning physics, *Geophysical Research Letter, Res.*, 102, 5929–5941, 1997.  
9  
10 Ridley, B., Pickering, K., and Dye, J.: Comments on the parameterization of lightning-  
11 produced NO in global chemistry-transport models, *Atmospheric Environment*, 39, 6184–6187,  
12 2005.  
13  
14 Rienecker, M. M., et al (2008), The GEOS-5 Data Assimilation System-Documentation  
15 of versions 5.0.1, 5.1.0, and 5.2.0. NASA/TM-2008-104606, Vol. 27, Technical Report Series  
16 on Global Modeling and Data Assimilation, 118 pp. (available at  
17 <http://gmao.gsfc.nasa.gov/systems/geos5/>)  
18  
19 Roof, C., Hansen, A., Fleming, G. G., Thrasher, T., Nguyen, A., Hall, C., Dinges, E., Bea, R.,  
20 Grandi, F., Kim, B. Y., Usdrowski, S., and Hollingsworth, P.: Aviation Environmental Design  
21 Tool (AEDT) System Architecture, Doc #AEDTAD-01, USDOT Volpe Center and CSSI Inc.  
22 and ATAC Inc. and Wyle Laboratories Inc. and Georgia Tech, Cambridge, MA, 2007.  
23  
24 Sillman, S., 2012. Overview: Tropospheric ozone, smog and ozone-NO<sub>x</sub>-VOC sensitivity.  
25 [online] University of Michigan. Available from: [http://www-](http://www-personal.umich.edu/~sillman/Sillman-webOZONE.pdf)  
26 [personal.umich.edu/~sillman/Sillman-webOZONE.pdf](http://www-personal.umich.edu/~sillman/Sillman-webOZONE.pdf) [Accessed 11 April 2012].  
27  
28 Spivakovsky, C. M., Logan, J. A., Montzka, S. A., Balkanski, Y. J., Foreman-Fowler, M.,  
29 Jones, D. B. A., Horowitz, L. W., Fusco, A. C., Brenninkmeijer, C. A. M., Prather M. J.,  
30 Wofsy, S. C., and McElroy, M. B.: Three-dimensional climatological distribution of

1 tropospheric OH: Update and evaluation, *J. Geophys. Res.*, 105, 8931–8980,  
2 doi:[10.1029/1999JD901006](https://doi.org/10.1029/1999JD901006), 2000.

3

4 Stevenson, D. S., and Derwent, R. G.: Does the location of aircraft nitrogen oxide emissions  
5 affect their climate impact? *Geophysical Research Letters* 36.17, L17810, 2009.

6

7 Stevenson, D. S., Doherty, R. M., Sanderson, M. G., Collins, W. J., Johnson, C. E., and  
8 Derwent, R. G.: Radiative forcing from aircraft NO<sub>x</sub> emissions: Mechanisms and seasonal  
9 dependence, *Journal of Geophysical Research*, 109, 2004.

10

11 Stevenson, D. S., Dentener, F. J., Schultz, M. G., et al.: Multi-model ensemble simulations of  
12 present-day and near future tropospheric ozone, *Journal of Geophysical Research*, 111,  
13 D08301, doi:[10.1029/2005JD006338](https://doi.org/10.1029/2005JD006338), 2006.

14

15 Tilmes, S., Lamarque, J.-F., Emmons, L. K., Conley, A., Schultz, M. G., Saunio, M., Thouret,  
16 V., Thompson, A. M., Oltmans, S. J., Johnson, B., and Tarasick, D.: Technical Note:  
17 Ozonesonde climatology between 1995 and 2011: Description, Evaluation and Applications,  
18 *Atmospheric Chemistry and Physics*, 12, 7475-7497, doi:[10.5194/acp-12-7475-2012](https://doi.org/10.5194/acp-12-7475-2012), 2012.

19 Voulgarakis, A., Savage, N. H., Wild, O., Carver, G. D., Clemitshaw, K. C., and Pyle, J. A.:  
20 Upgrading photolysis in the p-TOMCAT CTM: model evaluation and assessment of the role of  
21 clouds, *Geoscientific Model Development*, 2, 59-72, 2009.

22

23 Tilmes, S., Lamarque, J.-F., Emmons, L. K., Kinnison, D. E., Bardee, C., Deeter, M., Vitt, F.:  
24 Representation of chemistry in CAM4 and CAM5 in the Community Earth System Model  
25 (CESM1.2), in preparation.

26

27 Voulgarakis, A., Naik, V., Lamarque, J.-F., Shindell, D. T., Young, P. J., Prather, M. J., Wild,  
28 O., Field, R. D., Bergmann, D., Cameron-Smith, P., Cionni, I., Collins, W. J., Dalsøren, S. B.,  
29 Doherty, R. M., Eyring, V., Faluvegi, G., Folberth, G. A., Horowitz, L. W., Josse, B.,  
30 MacKenzie, I. A., Nagashima, T., Plummer, D. A., Righi, M., Rumbold, S. T., Stevenson, D.

1 S., Strode, S. A., Sudo, K., Szopa, S., and Zeng, G.: Analysis of present day and future OH and  
2 methane lifetime in the ACCMIP simulations, *Journal of Atmospheric Chemistry and Physics*,  
3 13, 2563–2587, doi:10.5194/acp-13-2563-2013, 2013.

4  
5  
6 Walcek, C. J., Brost, R. A., Chang, J. S., and Wesely, M. L.: SO<sub>2</sub>, sulfate and HNO<sub>3</sub> deposition  
7 velocities computed using regional land use and meteorological data, *Atmospheric*  
8 *Environment*, 20, 946–964, 1986.

9  
10 Walmsley, J. L. and Wesely, M. L.: Modification of coded parameterizations of surface  
11 resistances to gaseous dry deposition, *Atmospheric Environment*, 30, 1181–1188, 1996.

12  
13 Wesely, M. L. and Hicks, B. B.: A review of the current status of knowledge on dry deposition,  
14 *Atmospheric Environment*, 34, 2261–2282, 2000.

15  
16 Wild, O., Prather, M. J., and Akimoto, H.: Indirect long-term global cooling from NO<sub>x</sub>  
17 emissions, *Geophysical Research Letters*, 28, 1719-1722, 2001.

18  
19 Wilkerson, J.T., Jacobson, M. Z., Malwitz, A., Balasubramanian, S., Wayson, R., Fleming, G.,  
20 Naiman, A. D., and Lele, S. K.: Analysis of emission data from global commercial aviation:  
21 2004 and 2006, *Journal of Atmospheric Chemistry and Physics*, 10, 6391–6408, 2010.

22  
23  
24  
25  
26  
27  
28  
29

1 Table 1. Annual tropospheric mean burden of HO<sub>x</sub>, NO<sub>x</sub>, gaseous NO<sub>y</sub> and the ratios of OH :  
 2 HO<sub>2</sub> and NO<sub>x</sub> : NO<sub>y</sub> in both CAM5 and CAM4 for both the control run (\_c) and aviation NO<sub>x</sub>-  
 3 perturbed run (\_p).

4

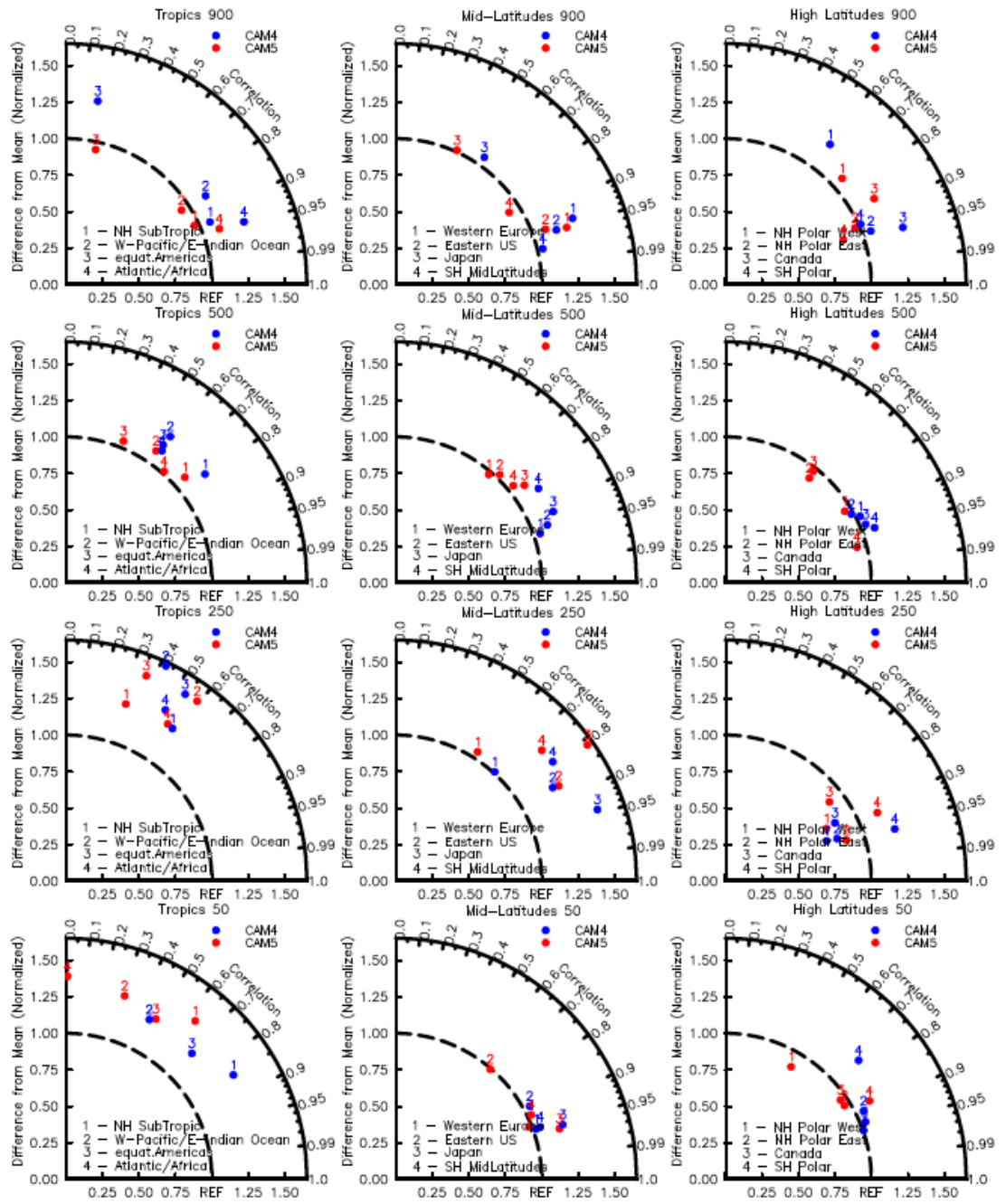
	O <sub>3</sub> (kg)	OH (kg)	HO <sub>2</sub> (kg)	HO <sub>x</sub> (kg)	OH/HO <sub>2</sub>	NO <sub>x</sub> (kgN)	NO <sub>y</sub> (kgN)	NO <sub>x</sub> /NO <sub>y</sub>
CAM4_c	3.71e+11	2.11E+05	2.59E+07	2.61E+07	8.15E-03	1.20E+08	7.69E+08	0.156
CAM4_p	3.79e+11	2.17E+05	2.58E+07	2.60E+07	8.39E-03	1.24E+08	7.96E+08	0.156
CAM5_c	3.41e+11	2.68E+05	2.73E+07	2.76E+07	9.82E-03	1.24E+08	7.30E+08	0.170
CAM5_p	3.50e+11	2.75E+05	2.72E+07	2.75E+07	1.01E-02	1.29E+08	7.73E+08	0.167

5 Table 2. Global annual average CH<sub>4</sub> lifetimes against reaction with OH, as calculated by CAM4  
 6 and CAM5 for the control run and for the NO<sub>x</sub> perturbation run. The relative change between  
 7 runs is displayed in the right-most column. It is noted that the calculated lifetimes are shorter  
 8 than the CH<sub>4</sub> lifetime derived based on Methyl chloroform analysis (Prather et al., 2012).

9

CH <sub>4</sub> lifetime (yr)	Control run	Perturbed run	Rel change (%)
CAM5	7.09	6.97	1.69
CAM4	8.83	8.71	1.40

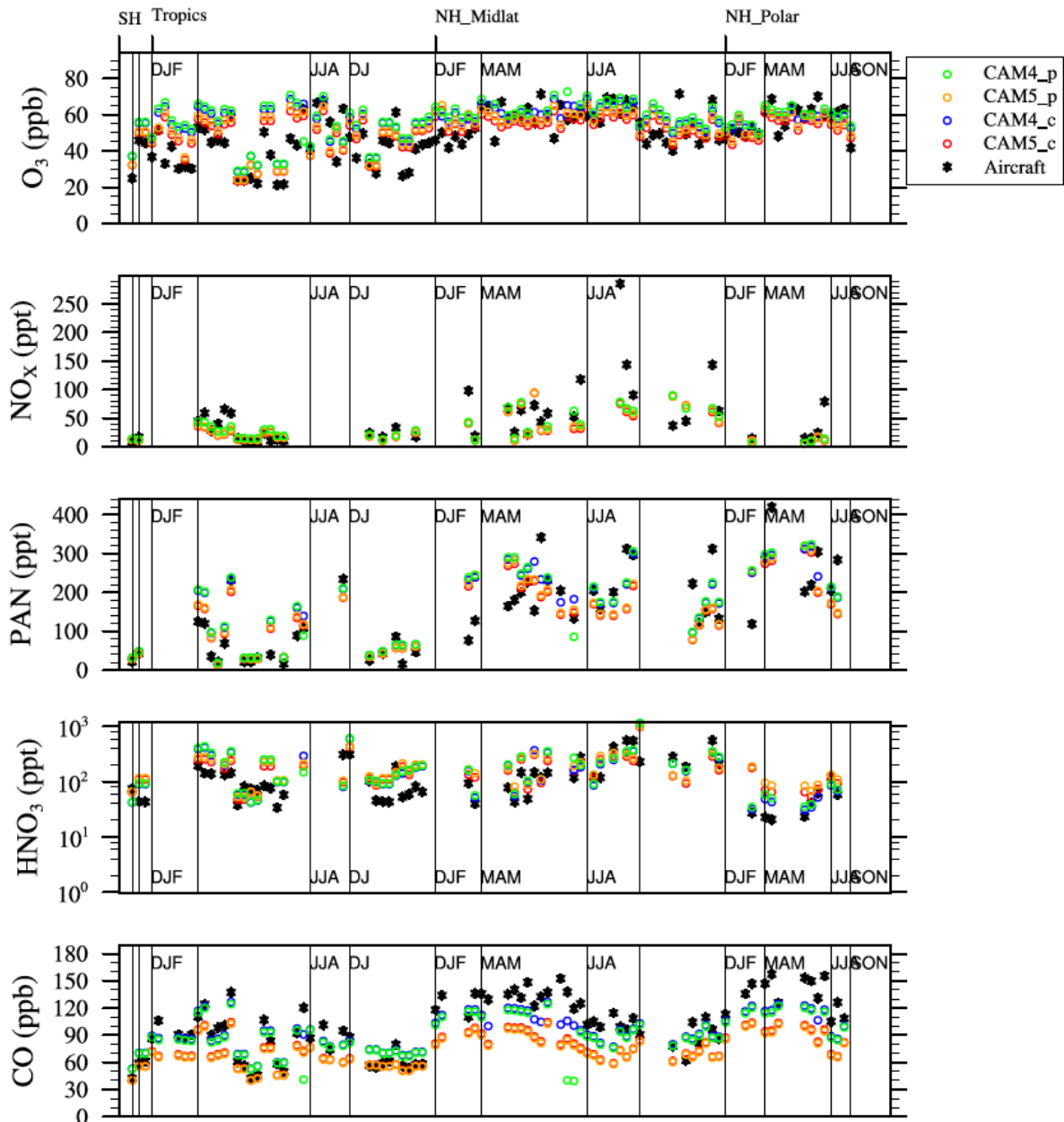
## Comparison to Ozonesondes



1

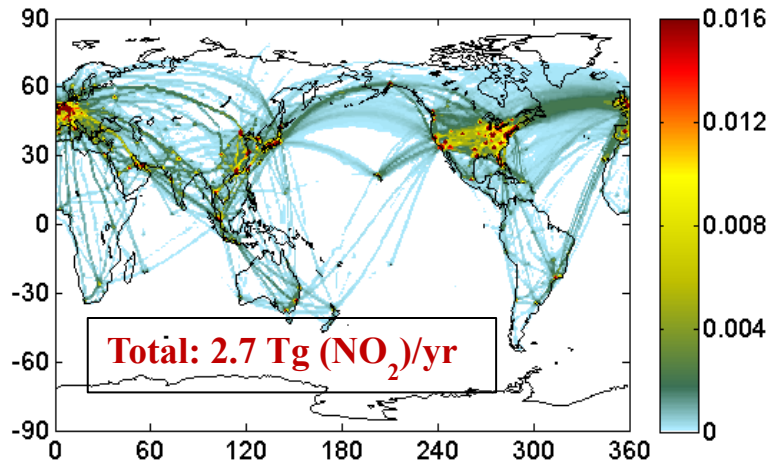
2 Figure 1. Taylor diagram of modeled background ozone from the control runs against  
 3 ozonesonde climatology for four pressure levels and three latitudinal regions. REF along the  
 4 abscissa denotes the observations while the radial distance describes the normalized bias. The  
 5 correlation for the seasonal cycle is described along the angle.





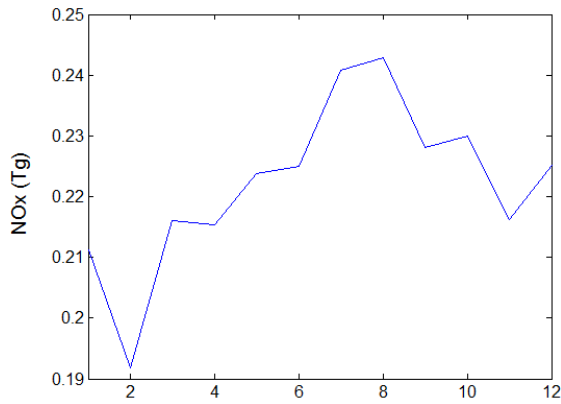
2 Figure 2. Comparison between aircraft observations over different regions and seasons and  
 3 different model simulation, averaged between 2-7km, for Ozone, NO<sub>x</sub>, PAN, HNO<sub>3</sub>, and CO,  
 4 based on an updated version of the aircraft climatology by Emmons et al., 2000, as described in  
 5 detail in Tilmes et al., 2014 (in preparation).

6



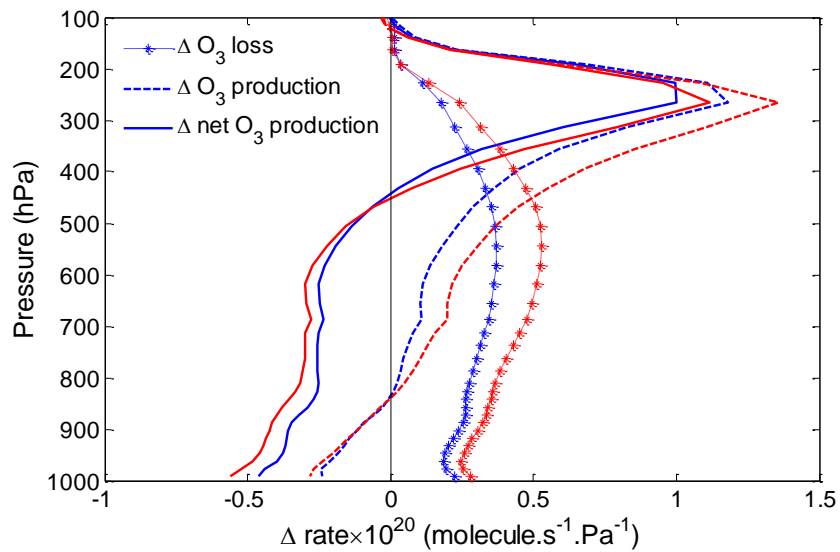
1  
2  
3

Figure 3. Spatial distribution of vertically-integrated aviation NO<sub>x</sub> emissions for 2006.



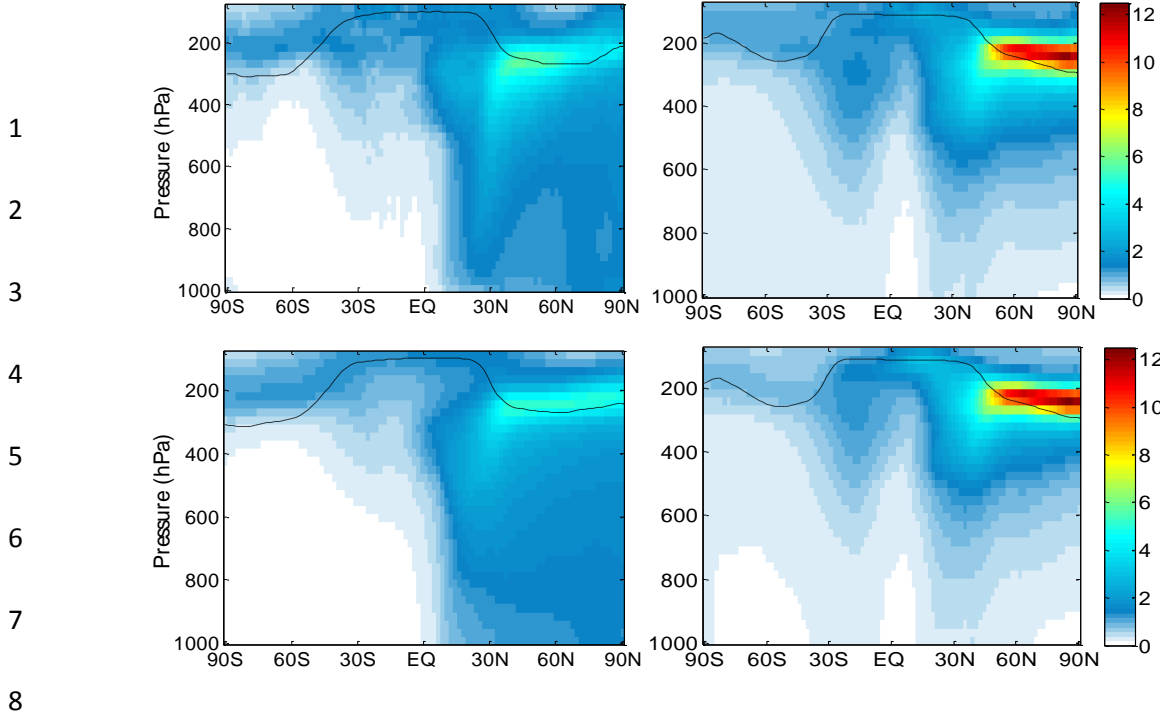
4

5 Figure 4. Seasonal distribution of global aviation NO<sub>x</sub> emissions for 2006.

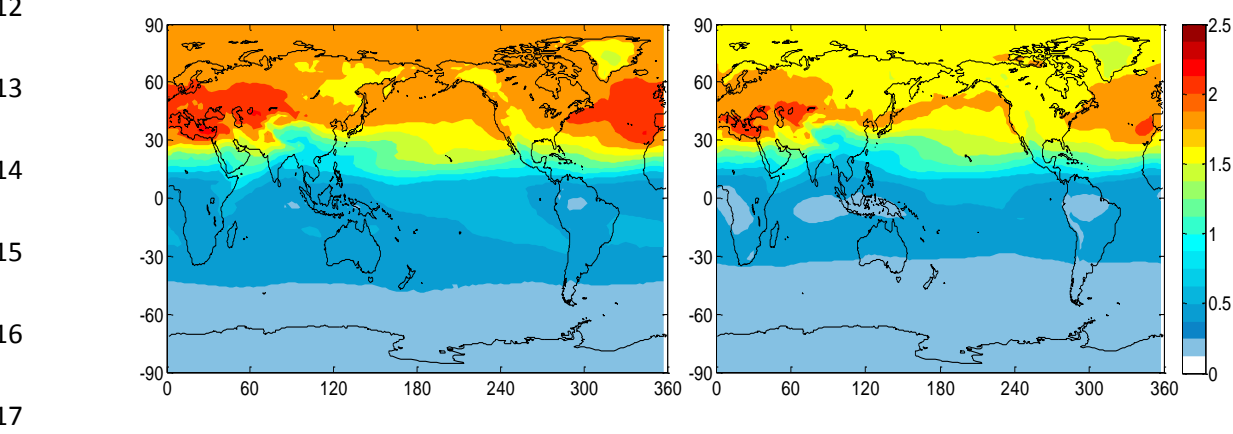


1

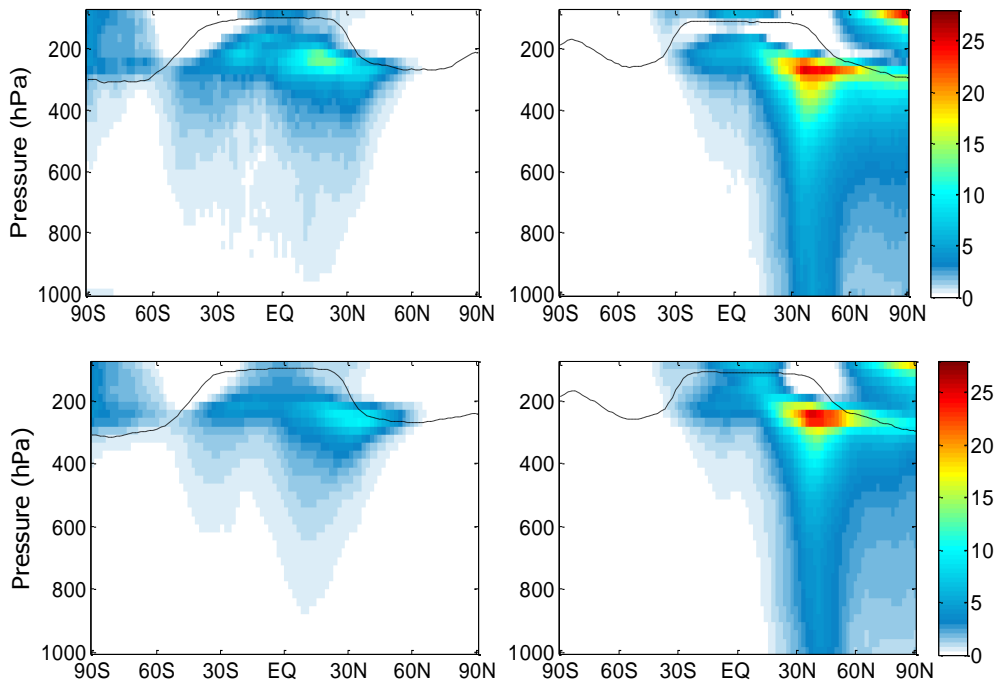
2 Figure 5. Vertical profile describing the aviation NO<sub>x</sub>-induced change in the rate of O<sub>3</sub>  
 3 production with height (results are shown in red for CAM5 and in blue for CAM4). Net rate of  
 4 ozone production (solid line), the gross rate of ozone production (dashed line), and the rate of  
 5 ozone loss (dotted line) are shown. Production and loss rates are calculated as zonal and  
 6 meridional means.



1  
2  
3  
4  
5  
6  
7  
8  
9 Figure 6. Zonal mean perturbations of ozone (ppb) during January (left) and July (right).  
10 CAM5 is in the top panel, while CAM4 is on the bottom. The dashed line indicates the  
11 tropopause.

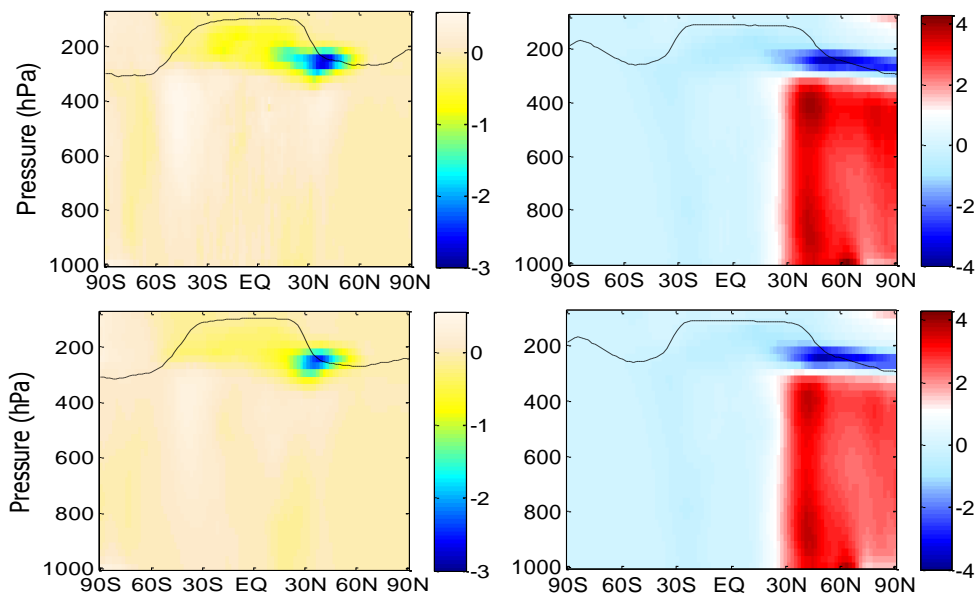


12  
13  
14  
15  
16  
17  
18 Figure 7. Yearly mean perturbations of the ozone column ( $\Delta$ DU) based on 2006 aircraft NO<sub>x</sub>  
19 emissions. CAM5 is on the left, while CAM4 is on the right.



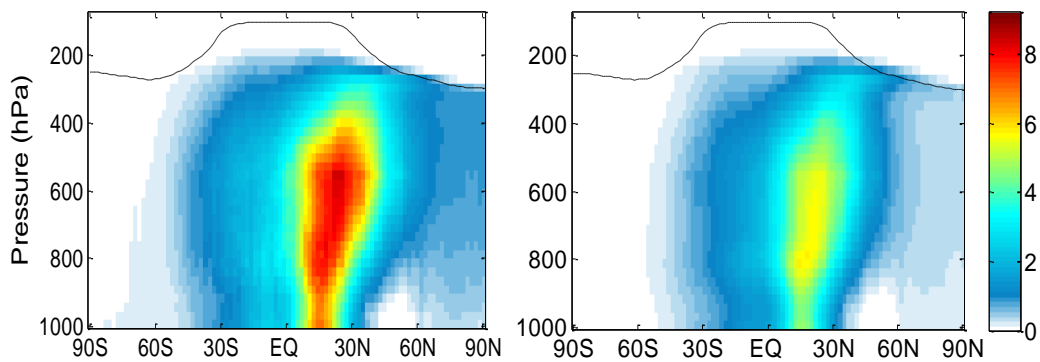
1  
2  
3  
4  
5  
6  
7

Figure 8. Aviation induced OH perturbations ( $10^{-4} \Delta\text{molec cm}^{-3}$ ) during January (left) and July (right). CAM5 is in the top panel, while CAM4 is in the bottom. The dashed line indicates the tropopause.



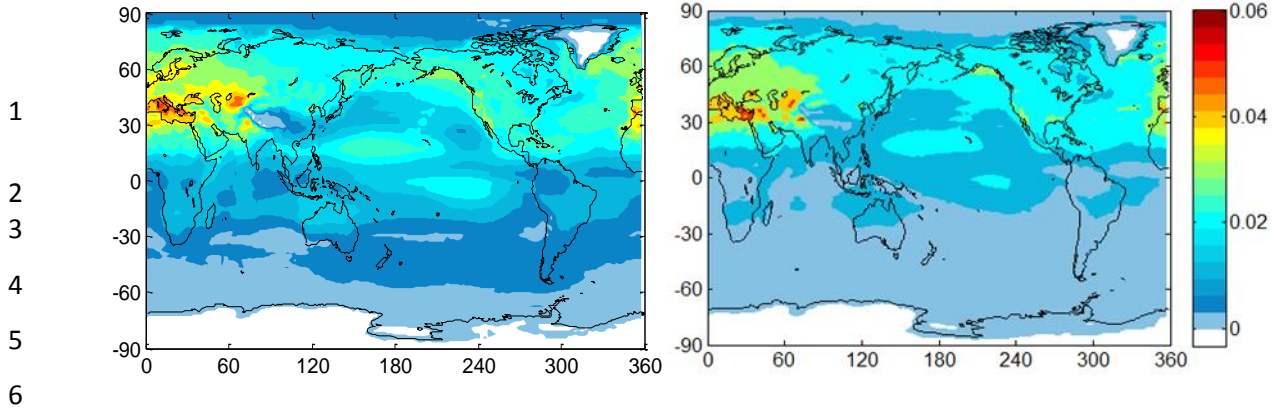
1  
2  
3  
4

Figure 9. As in Figure 7, but for HO<sub>2</sub> ( $10^{-6} \Delta\text{molec cm}^{-3}$ ).



5  
6  
7  
8  
9  
10  
11  
12  
13  
14  
15

Figure 10. Annual zonal averaged CH<sub>4</sub> loss ( $10^{-3} \Delta\text{molec cm}^{-3}\text{s}$ ) induced by aviation NO<sub>x</sub> emissions. CAM5 is on the left, CAM4 is on the right. The dashed line indicates the tropopause.



7 Figure 11. Yearly mean radiative forcing ( $\text{mWm}^{-2}$ ) from  $\text{O}_3$  due to aviation  $\text{NO}_x$  emissions.  
8 CAM5 is on the left, CAM4 is on the right.